BASTA, a 95 GHz FMCW Doppler radar for cloud and fog studies

Julien Delanoë*

Laboratoire ATmosphère, Milieux, et Observations Spatiales (LATMOS), Guyancourt, France

Alain Protat

Australian Bureau of Meteorology, Melbourne, Australia

Jean-Paul Vinson, Williams Brett, Christophe Caudoux, Fabrice Bertrand

Laboratoire ATmosphère, Milieux, et Observations Spatiales (LATMOS/UVSQ/CNRS/UPMC) Guyancourt, France

Jacques Parent du Chatelet, Ruben Hallali

Laboratoire ATmosphère, Milieux, et Observations Spatiales (LATMOS/UVSQ/CNRS/UPMC) Guyancourt and Météo-France, CNRS - CNRM-GAME, Centre National de Recherches Météorologiques, France

Laurent Barthes

Laboratoire ATmosphère, Milieux, et Observations Spatiales (LATMOS/UVSQ/CNRS/UPMC) Guyancourt, France

Martial Haeffelin and Jean-Charles Dupont

Institut Pierre Simon Laplace (IPSL) Palaiseau, France

[*]*Corresponding author address:* Laboratoire ATmosphère, Milieux, et Observations Spatiales (LATMOS), IPSL/UVSQ/CNRS/UPMC, Guyancourt, France

E-mail: julien.delanoe@latmos.ipsl.fr

ABSTRACT

Doppler cloud radars are amazing tools to characterize cloud and fog properties and to improve their representation in models. However commercially-available cloud radars (35 and 95 GHz) are still very expensive, which hinders their widespread deployment. In this study we present the development of a lower-cost semi-operational 95 GHz Doppler cloud radar called BASTA for Bistatic rAdar SysTem for Atmospheric studies. In order to drastically reduce the cost of the instrument a different approach is used compared to traditional pulsed radars: instead of transmitting a large amount of energy for a very short time period (as a pulse), a lower amount of energy is transmitted continuously. In the paper we show that using specific signal processing technique the radar can challenge expensive radars and provide high-quality measurements of cloud and fog. The latest version of the instrument has a sensitivity of about -50 dBZ at 1 km for 3 s integration and a vertical resolution of 25 m. BASTA radar currently uses four successive modes for specific applications: the 12.5 m vertical resolution mode is dedicated to fog and low clouds, the 25 m mode is for liquid and ice mid-tropospheric clouds and the 100 m and 200 m are ideal for optically-thin high-level ice clouds. We also highlight the advantage of such a radar for calibration procedures and field operations. The radar comes with a set of products dedicated to cloud and fog studies. For instance, cloud mask, corrected Doppler velocity and multi mode products combining high sensitivity mode and high resolution modes are provided.

1. Introduction

Doppler cloud radars are amazing tools to characterize cloud and fog properties and to improve their representation in models (Illingworth et al. 2007; Bouniol et al. 2010; Haeffelin et al. 2009; Maier et al. 2012; Dupont et al. 2012). Depending on the scientific application, they can be deployed from ground or ship (Moran et al. 1998; Kollias et al. 2007a), aircraft (Horie et al. 2000; Li et al. 2001; Wolde and Pazmany 2005; Delanoë et al. 2013; Hagen et al. 2014) or satellite (Stephens et al. 2002; Illingworth et al. 2015). The unique aspect of a Doppler cloud radar is its capability to describe at high vertical resolution (typically 50-100m) cloud properties from all types of clouds, from thin cirrus to rain or snow. The high-frequency cloud radars are however subject to attenuation in rain cases but they can still be used as long as the attenuation is corrected and not too strong (Lhermitte 1990). However despite these obvious advantages, cloud radars are currently not deployed in coordinated networks as are other instruments, such as radiation instruments and lidars (e.g. Illingworth et al. (2007). The reason for this is that commercially-available cloud radars are still very expensive (i.e. over 500 keuros), hampering their widespread deployment. In order to overcome this problem, we explore in this paper the development of a lower-cost semi-operational 95 GHz Doppler cloud radar. Most of the cost comes from the transmitter itself, as 95 GHz pulsed radars need to transmit typically 1-2 kW to achieve the sensitivity required for cloud and fog studies. In order to drastically reduce the cost of the instrument a different approach can be envisaged: instead of transmitting a large amount of energy for a very short time period (as a pulse), a lower amount of energy can be transmitted continuously. This technology is known as Frequency Modulated Continuous Wave (FMCW) (Ligthart et al. 1986; Yamaguchi et al. 2006; Huggard et al. 2008; Sami 2009; Williams 2011). Such FMCW radars have been developed in the past for a wide range of applications, such as the characterization of ocean waves (Hauser et al.

1992). Very few developments have been geared towards the characterization of clouds and fog (e.g., Yamaguchi et al. (2006); Huggard et al. (2008); Thies et al. (2010)). The main challenge of such a radar is to optimize the signal processing in order to compensate for the lack of power of the transmitter. Also, when a continuous signal is transmitted instead of a pulse, it becomes mandatory to find a way to ”tag” the signal in order to identify where the energy comes from and the phase difference to compute the Doppler spectrum. Also, receiving CW signals with an antenna very close to the transmitting antenna introduces additional challenges.In this paper we describe the FMCW radar project BASTA (Bistatic rAdar SysTem for Atmospheric studies) developed at the LATMOS (Laboratoire Atmosphres, Milieux, Observations Spatiales) and illustrate the potential of such a radar for cloud and fog studies. In section 2 we provide a general description of the BASTA radar and its applications. A technical description of the radar and the principle of this FMCW radar are then given in section 3. Section 4 describes the calibration aspect of the radar using different approaches. Comparisons of the BASTA radar against a state-of-the-art pulsed radar are discussed in section 5. Some remaining issues and technical points are presented in section 7. Conclusions and discussions on the next steps of this development are given in section 8.

2. General description of the BASTA concept and application

a. Main characteristics of the radars

After a long development process which started in 2006, the first prototype of BASTA has been deployed at SIRTA (Haeffelin et al. (2005)) in Palaiseau, France. This first prototype has operated continuously since 2010. The BASTA radar has even operated 100% of the time for the past two years. This illustrates the robustness of the design for potential operational deployment. Pictures of the instrument are shown in Fig.1, where panel A illustrates the bistatic configuration of the radar. The two Cassegrain dishes (60 cm in diameter) as well as all the electronic components are installed in a pressurized and insulated box (154 cm$\times$95 cm$\times$74 cm). The main characteristics of BASTA are given in Table 1. Power generators and the acquisition computer are stored in a shelter. Panel B shows the outside of the radar, when covered by its radome. It is to be noted that a simple plexiglass roof window is used instead of a very expensive radome. The performance of this radome fully satisfies the requirements. We estimated the two-way attenuation loss due to such a radome to be smaller than 3 dB by alternating measurements through a homogeneous cloud layer with and without the radome. Stickers are also used to protect the radar from direct solar radiation and to mitigate the green house effect during summer time. The radar uses a solid state transmitter (0.5 W) and measures both reflectivity and Doppler velocity. Building on the first prototype operating at SIRTA (BASTA-SIRTA), we developed a new generation of BASTA radars with very similar characteristics (Table 1) but with upgraded capabilities (slightly more powerful amplifier, i.e. 1 W). The first one (hereafter referred to as BASTA-BOM) belongs to the Australian Bureau of Meteorology. The second one (BASTA-MOBILE) is owned by LATMOS. Both are dedicated to field campaign deployments. The three radars share the same dimensions and weight (around 60 kg). Therefore they are easy to manipulate and move. BASTA-BOM and BASTA-MOBILE are almost identical.

b. Radar measurements and dynamic range

Fig.2 shows three weeks of continuous measurements of reflectivity (top panel) and Doppler velocity (bottom panel) at SIRTA as collected with the BASTA-MOBILE. A large variety of meteorological conditions and cloud types is observed, including low clouds, fog, cirrus and liquid precipitation. The vertical resolution is 25 m and the integration time is set to 3 s, with a maximum range of 12 km and a Nyquist velocity of 5 m/s. This example shows the capability of the radar to operate continuously for uninterrupted periods of time, and to detect all types of clouds with its sensitivity of about -44 dBZ at 1 km corresponding to this setup (sensitivity is discussed hereafter). Note that the background noise has been removed (see section d).

Fig.3 illustrates the statistical performances of the three radars (BASTA-SIRTA/BOM/MOBILE) at 25 m resolution and 3 s integration for different time periods. Left-hand panels (a to f) represent the probability distribution of the calibrated and range corrected reflectivity versus altitude. Only reflectivities above noise level are included. The noise level is determined using the furthest clear sky gate from the radar for each radial. In case there is no clear sky gate available a default value is used based on the latest available values. The BASTA-SIRTA distribution (panel a) is the accumulation of one year (2014) of data at SIRTA with the first prototype. Panel b shows statistics derived from 9 months of data collected with BASTA-BOM at Darwin airport from March to December 2014. Note that the reflectivity has not been corrected from gaseous attenuation. This panel illustrates the capability of BASTA radars to observe clouds up to 12 km. The BASTA-BOM was deployed at a tropical latitude (Darwin, Northern Australia), characterized by heavy precipitation during the wet season and a melting layer at about 5 km height. The small change in 0°C isotherm altitude during the wet season explains the sharp drop in reflectivity at 5 km. The altitude of the melting layer is not as readily observed in the midlatitude data given the comparably larger seasonal variability of the melting layer height. During the development phase of the two most recent radars, we carried out several direct comparisons between the prototype and the two other radars operating at the same time and place. A direct comparison of the performances of the BASTA-BOM radar against the first prototype is shown in panels c and d for the last ten days of January 2014 at SIRTA. Despite a small amount of data the better sensitivity of the BASTA-BOM radar is obvious, especially for high altitude clouds where the BASTA-BOM shows much more hits above 6 km. One month of data has been collected with BASTA-MOBILE at SIRTA (January 2015). The results are presented in panels e and f for the same period. BASTA-MOBILE, due to its better sensitivity, also exhibits more hits above 6 km with a difference in sensitivity larger that 10 dB. In order to better characterize the sensitivity and the measurement dynamics of the radars, the same distributions but normalized by the total number of measurements at a given altitude are shown on the right-hand panels of Fig.3, ie from g to l. Percentages smaller than 0.1% are not displayed. We estimate the overall sensitivity of each radar at 1 km as -35 dBZ, -49 dBZ and -44 dBZ for BASTA-SIRTA, BASTA-BOM and BASTA-MOBILE respectively for 3 s integration. These results (not shown) confirmed the statistical difference in sensitivity between the radars as observed in Fig.3. It is important to mention though that this sensitivity changes with atmospheric conditions and noise removing technique. Fig.3 also allows for an estimation of the dynamic range of these radars at 1 km. This dynamic range is about 42 dB, 60 dB and 55 dB for BASTA-SIRTA, BASTA-BOM and BASTA-MOBILE, respectively.

c. Four modes for different applications

Clouds in the troposphere are characterized by a variety of geometrical and optical thicknesses at different heights. Designing the most appropriate cloud radar parameters requires to take into account our current knowledge of these cloud properties. Given the range squared loss in sensitivity, it is much more challenging to detect thin cirrus clouds in the Tropics (found at ranges up to 18 km) than to detect drizzling stratocumulii. It is also crucial to detect some types of clouds with as high a vertical resolution as possible, in order to accurately characterize the altitudes of their base and top. It is particularly important for geometrically thin liquid cloud layers and fog. However, we cannot have both in one operating mode, as increasing range resolution readily comes at the expense of sensitivity.

As a result, cloud radars typically use more than one mode of operations. For instance, cloud radars deployed by the US Department of Energy (DOE) Atmospheric Radiation Measurement (ARM) program use a ”general” mode with intermediate sensitivity and range resolution, but also a ”precipitation” mode, a ”cirrus” mode using pulse compression, and a ”boundary layer” mode (Kollias et al. 2007b) to optimize the detection of these different types of clouds. Following this requirement that the detection of different types of clouds should be optimized, the BASTA radars use four distinct modes, characterized by different range resolutions: 12.5 m, 25 m, 100 m and 200 m. Radar characteristics of each mode are presented in Table 2. Since the integration time is set to 3 s for the modes, each mode is therefore repeated every 12 s. The real time processing is sufficiently fast to process data during the acquisition time. The 25 m resolution mode covers the range 125 m to 12 km with a sensitivity suitable to detect most low-level liquid clouds and thick cirrus. The 12.5 m resolution mode is dedicated to the low clouds, fog and precipitation. In this mode, the 6 dB loss in sensitivity relative to the 25 m mode is balanced by the closer range of fog and thin liquid clouds or the high reflectivity of rain. Also, this 12.5 m mode is limited to 6 km but the Nyquist velocity is extended to 10 m/s, which is particularly relevant for rain. This very high vertical resolution mode is ideal for fog and low stratus studies (Maier et al. 2012; Dupont et al. 2012).

Fig 4 shows two examples of low cloud/fog measurements. The first case is the evolution of a drizzling stratus sampled for over 70 h from the 21st of December 2014. The second one shows the life cycle of a persistent fog from the 5th of January 2015. The minimum range measurement for the 12.5 m mode is about 40 m for the Doppler velocity, which corresponds to three radar gates. Note that this short minimum distance measurement is a benefit from the bistatic nature of the instrument. Unfortunately we cannot use the very first gates due to coupling effect (i.e. direct interaction between the antennas at very close range). The reflectivity measured between 40 m and 240 m must be used with caution due to the beam overlap issue and the fact that the far field approximation is not valid (minimum 240 m at this wavelength with 60 cm dishes). Note that Sekelsky (2002) proposed a correction for the near near-field reflectivity.

The two other modes which are mainly dedicated to the detection of thinner cirrus clouds, 100 m and 200 m are 6 dB and 9 dB more sensitive than the 25 m mode, respectively. Fig.5 illustrates the four modes measurements for the 18th of January 2014 case with the BASTA-BOM radar at SIRTA during its test phase. The two top panels depict the range-corrected and calibrated reflectivity and Doppler velocity. We clearly see the impact of the mode on the sensitivity and the capacity to measure at very close range to the radar. From this example we observe a noise contamination from 10 UTC until the end of the day above 5 km for the 12.5 m mode.

This artifact can be easily removed using the information from the other modes. Note that this rise in the noise floor appears only if the meteorological signal is very strong in the vicinity of the radar and the meteorological target has a weak echo above this strong signal. This is due to the imperfections of one of the electronic parts (Single Side Band mixer defined later in the text) and the choice of the central chirp frequency. It does not affect all modes in the same way as it also depends on the frequency width of the chirp. We are currently investigating a solution to remove this artifact by changing the central chirp frequency. Note that it is possible to select 4 modes or one of them and the integration time from the radar control software.

d. Radar products

Radar products are currently developed for the BASTA radar, all relying on the same techniques as commonly used for pulsed radars. The background noise is first removed using a thresholding technique and the isolated pixels are removed using erosion image processing. The mean and standard deviation of the backscattered power signal at the far end of the radial is used to work out the threshold value to be used. In case of cloud contamination we use a reference value which has been derived from a longer monitoring of the noise characteristics for long clear sky periods preceding the current observation. Note that the background noise value is by definition the same for the four modes. This is crucial for the 12.5 m mode as the range bins at 6 km are much more likely to include cloud echoes than at 12 km in the midlatitudes. We also use a structure recognition technique based on the standard deviation of the Doppler velocity in a running window. The velocity offers a higher contrast than the reflectivity. The Doppler velocity varies within the range [-V_{max},+V_{max}], where V_{max} is the Nyquist velocity. As a result if the droplet velocity is faster than V_{max}, the velocity will be folded within that range. Fortunately, the unfolding process is straightforward. We use a gate to gate correction initialized at the first gate by the measured value, assuming that most of the time the vertical air velocity is small near the ground, and as a result the Doppler velocity is almost equal to the reflectivity-weighted terminal fall speed. We can also use the rain detection to check the sign of the velocity. The 25 m, 100 m and 200 m modes have a Nyquist velocity of around 5 m/s. In very ambiguous cases we use the velocity measured by the 12.5 m mode (for which $V_{max} \approx$10 m/s) to unfold Doppler velocity from the other modes.

We also developed a synergistic product which combines all modes, so that non expert users can readily use a single reflectivity and Doppler velocity estimate. In order to construct this product, the 25 m mode is used as a baseline. The 12.5 m measurements are then averaged at the resolution of the other modes and used to correct the folded Doppler velocities of the other modes. The most sensitive modes (100 m and 200 m) are oversampled onto the 25 m resolution grid. An illustration of this radar product is given in Fig. 6, where the top panel shows the multi mode reflectivity and the middle panel shows the Doppler velocity measured on the 19th of January 2014 at SIRTA using the BASTA-BOM radar. The bottom panel indicates from which mode the information comes from. A dedicated fog product is also similarly derived at the 12.5 m resolution, using the 12.5 m mode as the baseline, and oversampling the other modes at this resolution. A detection of the melting layer is also available in case of stratiform rain (not shown). Several radar-only algorithms will also be adapted in a near future to derive ice/liquid water content and more cloud microphysical properties from the BASTA observations (Matrosov and Heymsfield 2000; Hogan et al. 2006; Deng and Mace 2006; Protat et al. 2007; Delanoë et al. 2007). The BASTA radar can also be combined with lidar and microwave radiometers to improve the accuracy of the cloud microphysical products (Löhnert et al. 2001; O'Connor et al. 2005; Illingworth et al. 2007; Delanoë and Hogan 2008).

3. Technical description and principle of the radar

a. Frequency Modulated Continuous Wave principle

Basically all radars work on the time delay between the transmitted wave and the received wave while the latter is travelling at the speed of light. This information is obtained by correlating the transmitted and backscattered signals. The signal processing allows one to compute the energy backscattered by the radar target but also to determine if the observed target is moving towards or away from the radar. This processing is clearly facilitated by using a wave packet (usually referred to as "pulses"), where energy is released for short time periods interleaved with silent periods. Since we know exactly which wave packet has been interacting with the target the range determination becomes obvious. Note that the pulse repetition frequency (PRF) and the pulse length define the performance and capability of the radar (ambiguous distance, ambiguous velocity, blind zone). Unfortunately the pulse approach requires the emission of a huge amount of energy for a very short period of time, which requires a very expensive transmitter (typically 250 keuros for 1.5 kW). The FMCW technique relies on the same radar principle except that the energy is transmitted continuously without any dead time. The pulse is replaced by a modulation of the radar frequency. Consequently most of the challenge with such radars lies in the signal processing. Fig. 7 describes the principle of the FMCW radar. The radar frequency varies between $F_0 - \Delta F$ and $F_0 + \Delta F$, where F_0 is the central frequency and ΔF represents half of the frequency band. A linear chirp is used to control the radar frequency changes. For example the red chirp corresponds to the transmitted signal and covers the $F_0 - \Delta F$ and $F_0 + \Delta F$ range in T_{rep} time. Once we get a return from the target the radar receives the echo signal in blue. The signal backscattered by the target is received with a time delay T_p, this time delay corresponds to a distance D which is defined by the following equation:

$$D = T_p \times \frac{c}{2} \tag{1}$$

where c is the electromagnetic-wave propagation speed. After convolution of the emitted and received signals, T_p is associated to a beat frequency F_b as shown in Fig. 7 such that:

$$F_b = 2\Delta F \times \frac{T_p}{T_{rep}} \tag{2}$$

Note that in our system the acquisition starts at $T_a = T_{rep}/2$ in order to avoid discontinuities due to extra echo returns as shown in the grey box included in Fig. 7. We clearly see the interest of using only half of the chirp as we avoid the contamination from other chirps (grey circle). Note that it does not suppress the contamination from target exceeding the maximum range however the return is weak enough to remain invisible. As a result there is a loss in sensitivity of 3 dB but we noticeably reduce typical FMCW artifacts. These artifacts, created by chirp returns, results in a frequency discontinuity and consequently in an increase of background noise within the radial. As a result the whole profile is contaminated and cannot be used.

As with any radar we can then compute:

- the ambiguous distance (D_a) :

$$D_a = T_a \times \frac{c}{2} \tag{3}$$

- the ambiguous velocity:

$$V_a = \frac{c}{4 \times F_0 \times T_{rep}} \tag{4}$$

- and the range resolution:

$$r = \frac{c}{2 \times 2\Delta F}. \tag{5}$$

Each mode is characterized by a dedicated chirp, i.e. a central frequency and a half band width.

b. BASTA radar technical description

The BASTA radar operates at 94.95 GHz. At such high frequency the radio frequency (RF) components are either not available or very expensive. Fortunately, RF sources are available and much cheaper at a lower frequency. As a result, we use a source at 15.825 GHz for the BASTA radar, as explained in what follows. Note that in that case the central frequency of the chirp (F_0) is not at 94.95 GHz. The radar diagram is presented in Fig 8. The technical description can be separated into three parts: the transmitter, the receiver, and the acquisition/signal processing.

1) TRANSMITTER CHAIN

The frequency modulated signal is generated from two signals. First, a single side band mixer (SSB) is triggered using a chirp frequency (F_{chirp}). It allows one to up convert a stabilized source frequency at 15.825 GHz to a F_1 frequency as shown in Fig 8. F_1 in GHz is defined as follow:

$$F_1 = 15.825 + F_{chirp}, \tag{6}$$

with $F_{chirp} = F_c \pm dF$. F_c is the central frequency and dF is defined as the half band width of the chirp. Then the second step of the signal generation makes use of a multiplier. F_1 is multiplied by 6 to obtain F_0. The derived signal is amplified (amplifier 0.5 W or 1W) and transmitted to the antenna via the wave guides. As a result F_0 can be expressed as:

$$F_0 = 6 \times F_1 = 94.95 + 6 \times F_{chirp} = 94.95 + 6F_c \pm \Delta F, \tag{7}$$

where $\Delta F = 6dF$.

2) Receiver chain

The receiver chain is based on a single down conversion. The received signal is amplified through the low noise amplifier (LNA). The received signal is mixed with a signal at 94.95 GHz obtained from the source at 15.825 GHz multiplied by 6. The derived signal IF, defined as :

$$IF = 6F_c \pm \Delta F, \tag{8}$$

is amplified and filtered.

3) Acquisition and signal processing

The analog signal IF from the receiver chain is digitized. The signal processing step is illustrated in Fig 9. It is based on the impulse response (R, complex number) in frequency in both module and phase for different radials. The impulse response is the result of a numerical demodulation of received chirp ($Chirp_{received}$) and its theoretical complex copy ($Chirp_{reference}$) weighted by a Hanning window which is a good compromise between frequency resolution and spectral leakage:

$$R = FFT[Chirp_{received} \times Chirp_{reference} \times Hanning]. \tag{9}$$

At this stage, the output signal is similar to a signal derived from a pulsed radar. The reflectivity and Doppler velocity are proportional to the module and the argument of a complex number PPP, respectively. PPP is computed using pulse pair processing following this expression:

$$PPP = \frac{1}{n-1} \sum_{i=0}^{i=n-1} R_i \times R_{i+1}^{*}, \tag{10}$$

where * refers to the complex conjugate of the impulse response. A field-programmable gate array (FPGA) is in charge of the acquisition and the signal processing. The main advantage of this system is the real time processing capability.

4. Calibration

Although cloud detection does not require any calibration, it is a crucial issue for the retrieval of cloud microphysical properties (such as liquid or ice water content). There are different ways to calibrate a cloud radar: knowing exactly all the constants and variables described in the radar equation (internal calibration) or using meteorological or metal targets of reference (external calibration). Unfortunately it remains very difficult to determine the exact power budget through electronic components and various gains. Therefore the target approach (artificial or meteorological) remains the best way to calibrate radars. For calibration purposes we benefit from the small size, light weight, and narrow beam width (0.4°) of the BASTA radar. The radar can be mounted on a swing system to point manually horizontally or at different elevations. This is illustrated in Figures 1c and d. On the 25th of June 2013 we carried out the first calibration procedure with the radar prototype (BASTA-SIRTA). The radar was on a shelter roof at 3 m above the ground and pointing towards a trihedral target, with a known backscatter, set at 560 m distance and mounted on a 20 m tall mast. In Fig 10 we illustrate the measurements collected for a few hours on that day. Panel a show the average power profile measured by the radar between 0 and 1 km, grey lines represent the standard deviation envelope. Similarly the panel b shows the average velocity profile. Note that during that period the relative humidity was less than 45 % and led to a two way atmospheric attenuation at 95 GHz smaller than 0.5 dB between the radar and the target. We clearly distinguish the target return for two gates (550 and 575 m) with a maximum power return between 212 and 214 (Fig 10a and c) in arbitrary unit (decibel). Note that trees are also backscattering the waves. However the Doppler velocity is not equal to zero contrary to the trihedral target due to the trees' motion (Fig 10b). The measurements were made using the 25 m resolution mode. It is then possible, knowing the theoretical return of the corner reflector, to evaluate the calibration value to convert the uncalibrated power measured by the radar into reflectivity value in dBZ.

Note that the other modes are calibrated using this value and taking into account the range resolution. BASTA-BOM and BASTA-Mobile have been calibrated using the BASTA-SIRTA as reference. The evolution of the calibration value is not presented in this study but will be thoroughly assessed in a future study. It is obvious that such a measurement must be repeated many times a year. Fortunately we will see in the next section that the value presented here is a very good proxy.

Hogan et al. (2003) proposed an elegant technique to calibrate 95 GHz radar and we have reproduced the same experiment using simultaneous measurements from BASTA-SIRTA (vertically pointing, Fig 1b) and BASTA-mobile at 30° elevation (Fig 1e) at the SIRTA observatory. Rain rate was measured during a rain event by the Dual-Beam Spectropluviometer (DBS, Delahaye et al. (2006)) which has been developed at LATMOS and operated at SIRTA only a few meters away from the radars. The concept of the Hogan et al. (2003) calibration technique is to simultaneously measure radar reflectivity at 500 m range and rain rate in light rain, and to compare the obtained relationship between these two measurements to that predicted assuming a shape for the rain drop size distribution and assuming that the path attenuation over a few hundred meters in light rain is small or corrected from attenuation. Note that in that case the radome must remains as dry as possible to avoid attenuation due to the wet radome. Hogan et al. (2003) positioned their radar at a 30° elevation and protected the radome using a shelter. The same protocol is repeated here with the BASTA-mobile tilted at 30° elevation and the radome protected from rain as shown in Fig 1e).

Fig 11 shows the data collected for two rain events (6th and 8th of October 2014). The average calibrated reflectivity at about 300 (panel a, inclined) and 500 m (panel b, vertical) of both radars are plotted against the rain rate. The distances used correspond to the same altitude accounting for the 30° elevation. Note that we assume that the difference in attenuation is small (compared to the wet radome attenuation) and we consider that the rain field is horizontally homogeneous within a few hundred meters. Green lines represent the averaged values of reflectivity in 0.2 mm/h bins of rain rate and the translucent lines indicate the standard deviation envelope. Circles and stars lines correspond to the vertical radar with wet radome and inclined radar with dry radome respectively. The red circle line illustrates the result of the attenuated reflectivity simulation at 500 m using drop size distribution measured by the DBS and the T matrix calculation assuming an aspect ratio as a function of the diameter (Beard and Chuang 1987). The difference between the dry radome measurement and T-matrix simulation for rain rate larger than 2 mm/h varies between 0.5 and 2 dB. The poor comparison between reflectivity simulation and measurements below 2 mm/h could be explained by the fact that the rain field is less homogenous and affected more significantly by the vertical air motion for the DBS measurements. For a proper calibration exercice we would recommend to increase the number of rain events to enlarge the statistic. The second very important result is the effect of the wet radome, with the attenuation reaching almost 20 dB. Note that these estimates of wet radome attenuation could be used as a proxy to correct the radar reflectivity as a function of rain rate, however this would require a specific study with numerous rain conditions. We want to stress here that both radomes have a very similar behavior with regards to the wet radome attenuation and the radars have been intercalibrated.

5. Comparison with pulsed radar

The BASTA-BOM radar was deployed at Darwin (Australia, NT) in March 2014. For 8 months the BASTA-BOM was operated alongside the DOE ARM Ka-Band Zenith Radar (KAZR) at 34.86 GHz. We do not intend to present here an extended comparison of the radars, which will be the subject of further investigation. Rather, here we illustrate the performance of the BASTA on one selected cirrus case with no underlying liquid cloud layer to avoid differences due to differential attenuation at the two frequencies in liquid clouds. We also intentionally chose a drier day to minimize the impact of the gaseous attenuation correction at the two frequencies. The gaseous attenuation at 35 GHz and 95 GHz have been estimated using the nearest sounding and the Liebe (1985) model. Figs. 12a and b show the KAZR reflectivity on the 17th of March 2014 using the most sensitive mode (chirp mode) and the general mode. Note that although the KAZR measurements (chirp mode) start at 1800 m and go up to 18 km, the comparison is limited to a maximum height of 12 km, which corresponds to the unambiguous range of BASTA in its current configuration. Figs. 12c, d and e show the same cloud observed by BASTA at 25 m, 100 m, and 200 m, respectively. For that specific day the difference in the two way attenuation is estimated at 1.5 dB at 12 km. The reflectivity of the radars has been corrected from gaseous attenuation. Note that the echoes observed by the KAZR below 2 km between 10 UTC and 14 UTC and not by BASTA are coming from insects (Wood et al. 2009); due to their large size and their rather small concentration the 35 GHz radar is more sensitive to their presence. There is clearly excellent agreement between the pulsed radar and FMCW radar observations of this ice cloud. Two periods are selected, between 12 and 14 UTC and between 14.5 and 15.5 UTC, where all the profiles are averaged and presented in Fig 12f and g. In theses profiles we clearly measure the sensitivity difference between the BASTA modes and the KAZR general and sensitive modes in the clear air part of these profiles. In that specific case, the differences in sensitivity between the BASTA 25 m, 100 m and 200 m modes and the sensitive KAZR mode (cirrus mode) are 19 dB, 13 dB and 10 dB, respectively. The difference in sensitivity between the BASTA 25 m and the general KAZR mode is around 2 dB. The sensitivity at 1 km of the BASTA-BOM at 25 m resolution is about -48 dBZ. A new mode dedicated to the Tropics is currently under development. This extra capability will profile the atmosphere at 100 m resolution with an unambiguous range at 18 km and an unambiguous velocity of 2.5 m/s.

6. Remaining issues and technical points

We made significant progress since the beginning of the project in 2006. For instance we abandoned the random code approach to use a chirp for modulating the signal. We also accepted to lose 3 dB sensitivity by using only half of the chirp, which has proven very efficient to mitigate typical FMCW signal contamination. In addition, many minor adjustments and improvements led to the encouraging results presented in this study. However a few artifacts remain in case of heavy rain, such as noise increase at the far end of the profile. This can be easily removed using post processing algorithms. We are currently working on a solution to get rid of these artifacts associated with heavy rain, by changing the central frequency of the chirp (IF). It is also important to mention that the FMCW radar is sensitive to external electromagnetic perturbation. For instance it is crucial to ensure that the cables between the radar box and the shelter are properly isolated. The coupling effect between the antennas can also introduce artifacts and we have limited their effects by using absorbing foam around and between the antennas and on the radar box frame. Having a bi-static radar have advantages as we can do measurements at very short range to the radar. However it is mandatory to accurately align the antennas in order to maximise beams overlap. To facilitate this setting the transmitting antenna is fixed and the receiving one can be adjusted using small elevators. For example we use the signal of an homogenous cirrus and adjust the receiving antenna until the received power is maximized.

7. Conclusion and outlook

In this paper we describe the BASTA cloud radar project, for which the FMCW technique is preferred to very expensive pulsed cloud radars. Since the development of the first prototype operating continuously at SIRTA since 2010, we have improved the system and built two other radars with outstanding performance. The first target of BASTA radar was the midlatitude clouds, therefore the maximum range was set to 12 km. The recent deployment of the instrument in the Tropics showed that given the high sensitivity of the BASTA radar the maximum range had to be extended to 20 km. Consequently we are developing a new mode at 100 m resolution with a more adequate maximum range. In this mode the unambiguous velocity will be 2.5 m/s instead of 5 m/s. The other modes will help to correct the folding issue in the common range. The pulse pair processing is currently done in the FPGA. We are investigating the capability to record the signal after the FFT complex calculation in order to carry spectrum analysis. This can be very useful for cloud phase discrimination (Shupe et al. 2004; Luke et al. 2010), turbulence studies (Brewster and Zrnić 1986), attenuation correction and drop size distribution retrieval (Giangrande et al. 2010). We demonstrate that the BASTA radar is a very promising alternative to the very expensive cloud radars. As the price remains reasonable it can be envisioned to develop networks of FMCW cloud radars. For instance, fog monitoring feasibility at airports using BASTA radar is currently underway. We are also experimenting the possibility to use a BASTA radar for studying volcanic ash (Donnadieu et al. 2011; Donnadieu 2012).

Some recent experiments have been carried with the objective of analyzing whether or not the refractivity variability measured with W-band radar can lead to information at hectometer scales on turbulent behavior of the atmosphere. BASTA was one of the radars used during a recent campaign which took place in France at SIRTA in summer 2014. The radar was pointing horizontally toward four calibrated targets and measured the refractivity variations during two months with a sampling rate of 0.25 s. Several instruments allowed comparison between radar refractivity measured by BASTA and in-situ measurements (using Besson et al. (2012)).

Acknowledgments. We are grateful to the SIRTA team which provides day to day basis support for operating the radars and organizing the data stream. We would like to express our thanks to Nicolas Pauwels and Christophe Legac for their help and for our fruitful discussions around FMCW technique. We also thank Brad Atkinson for his help with the installation of BASTA-BOM in Darwin. We would like to thank "U.S. Department of Energy as part of the Atmospheric Radiation Measurement Climate Research Facility" for providing KAZR data. BASTA developments have been partly funded by CNES, INSU, Ecole Polytechnique and Région Ile de France. We would like to acknowledge ACTRIS and PARIFOG projects. Julien Delanoë's research is partly funded by CNES.

References

Beard, K. V., and C. Chuang, 1987: A new model for the equilibrium shape of raindrops. *J. Atmos. Sci.*, **44**, 1509–1524.

Besson, L., C. Boudjabi, O. Caumont, and J. Parent du Châtelet, 2012: Links between refractivity characteristics and weather phenomena measured by precipitation radar. *Bound-Lay Meteor*, **143**, 77–95.

Bouniol, D., and Coauthors, 2010: Using Continuous Ground-Based Radar and Lidar Measurements for Evaluating the Representation of Clouds in Four Operational Models. *Journal of Ap-*

plied Meteorology and Climatology, **49 (9)**, 1971–1991, doi:10.1175/2010JAMC2333.1, URL http://dx.doi.org/10.1175/2010JAMC2333.1.

Brewster, K. A., and D. S. Zrnić, 1986: Comparison of eddy dissipation rates from spatial spectra of Doppler velocities and Doppler spectrum widths. *Journal of Atmospheric and Oceanic Technology*, 440–452.

Delahaye, J.-Y., L. Barthès, P. Golé, J. Lavergnat, and J. P. Vinson, 2006: A dual-beam spectro-pluviometer concept. *J. Hydrol.*, **328**, 110–120, doi:10.1016/j.jhydrol.2005.11.048.

Delanoë, J., and R. J. Hogan, 2008: A variational scheme for retrieving ice cloud properties from combined radar, lidar and infrared radiometer. *J. Geophys. Res.*, **113**, D07204, doi:10.1029/2007JD009000.

Delanoë, J., A. Protat, O. Jourdan, J. Pelon, M. Papazzoni, R. Dupuy, J.-F. Gayet, and C. Jouan, 2013: Comparison of Airborne In Situ, Airborne Radar–Lidar, and Spaceborne Radar–Lidar Retrievals of Polar Ice Cloud Properties Sampled during the POLARCAT Campaign. *Journal of Atmospheric and Oceanic Technology*, **30 (1)**, 57–73, doi:10.1175/JTECH-D-11-00200.1, URL http://dx.doi.org/10.1175/JTECH-D-11-00200.1.

Delanoë, J., A. Protat, J. Testud, D. Bouniol, A. J. Heymsfield, A. Bansemer, and P. R. A. Brown, 2007: The characterization of ice clouds properties from Doppler radar measurements. *J. Appl. Meteorol. Climatology*, **46**, 1682–1698, doi:10.1175/JAM2543.1.

Deng, M., and G. G. Mace, 2006: Cirrus Microphysical Properties and Air Motion Statistics Using Cloud Radar Doppler Moments. part i: Algorithm Description. *Journal of Applied Meteorology and Climatology*, **45 (12)**, 1690–1709, doi:10.1175/JAM2433.1, URL http://dx.doi.org/10.1175/JAM2433.1.

Donnadieu, F., 2012: *Volcanological Applications of Doppler Radars: A Review and Examples from a Transportable Pulse Radar in L-Band*. InTech, 409-446 pp., doi:10.5772/35940.

Donnadieu, F., S. Valade, and S. Moune, 2011: Three dimensional transport speed of wind-drifted ash plumes using ground-based radar. *Geophys. Res. Lett.*, **38 (L18310)**.

Dupont, J.-C., M. Haeffelin, A. Protat, D. Bouniol, N. Boyouk, and Y. Morille, 2012: Stratus fog formation and dissipation. a 6-day case study. *Boundary-Layer Meteorology*, **143**, 207–225.

Giangrande, S. E., E. Luke, and P. Kollias, 2010: Automated Retrievals of Precipitation Parameters Using Non-Rayleigh Scattering at 95 GHz. *Journal of Atmospheric and Oceanic Technology*, **27**, 1490–1503, doi:10.1175/2010JTECHA1343.1.

Haeffelin, M., and Coauthors, 2005: SIRTA, a ground-based atmospheric observatory for cloud and aerosol research. *Annales Geophysicae*, **23**, 253–275.

Haeffelin, M., and Coauthors, 2009: Parisfog: Shedding new light on fog physical processes. *Bulletin of the American Meteorological Society*, **91 (6)**, 767–783, doi:10.1175/2009BAMS2671.1, URL http://dx.doi.org/10.1175/2009BAMS2671.1.

Hagen, M., and Coauthors, 2014: Airborne remote sensing of cloud properties with the german research aircraft HALO. *8th European Conference on Radar in Meteorology and Hydrology*.

Hauser, D., G. Caudal, G. Rijckenberg, D. Vidal-Madjar, G. Laurent, and P. Lancelin, 1992: Ressac: a new airborne FM/CW radar ocean wave spectrometer. *Geoscience and Remote Sensing, IEEE Transactions on*, **30 (5)**, 981–995, doi:10.1109/36.175333.

Hogan, R. J., D. Bouniol, D. N. Ladd, E. J. O'Connor, and A. J. Illingworth, 2003: Absolute Calibration of 94/95-GHz Radars Using Rain. *Journal of Atmospheric and Oceanic*

Technology, **20 (4)**, 572–580, doi:10.1175/1520-0426(2003)20⟨572:ACOGRU⟩2.0.CO;2, URL http://dx.doi.org/10.1175/1520-0426(2003)20⟨572:ACOGRU⟩2.0.CO;2.

Hogan, R. J., M. P. Mittermaier, and A. J. Illingworth, 2006: The retrieval of ice water content from radar reflectivity factor and temperature and its use in evaluating a mesoscale model. *Journal of Applied Meteorology and Climatology*, **45 (2)**, 301–317, doi:10.1175/JAM2340.1, URL http://dx.doi.org/10.1175/JAM2340.1.

Horie, H., H. Okamoto, S. Iwasaki, H. Kumagai, and H. Kuroiwa, 2000: Cloud observation with CRL airborne cloud profiling radar (SPIDER). *Geoscience and Remote Sensing Symposium, 2000. Proceedings. IGARSS 2000. IEEE 2000 International*, Vol. 1, 190–191 vol.1, doi:10.1109/IGARSS.2000.860464.

Huggard, P. G., and Coauthors, 2008: 94 GHz FMCW cloud radar. *Proc. SPIE 7117, Millimetre Wave and Terahertz Sensors and Technology*, **7117**, doi:10.1117/12.800347.

Illingworth, A. J., and Coauthors, 2007: Cloudnet - continuous evaluation of cloud profiles in seven operational models using ground-based observations. *Bull. Am. Meteorol. Soc.*, **88**, 883–898.

Illingworth, A. J., and Coauthors, 2015: The EarthCARE Satellite: The Next Step Forward in Global Measurements of Clouds, Aerosols, Precipitation, and Radiation. *Bulletin of the American Meteorological Society*, **96 (8)**, 1311–1332, doi:10.1175/BAMS-D-12-00227.1, URL http://dx.doi.org/10.1175/BAMS-D-12-00227.1.

Kollias, P., E. E. Clothiaux, M. A. Miller, B. A. Albrecht, G. L. Stephens, and T. P. Ackerman, 2007a: Millimeter-wavelength radars: New frontier in atmospheric cloud and precipitation research. *Bulletin of the American Meteorological Society*, **88 (10)**, 1608–1624, doi: 10.1175/BAMS-88-10-1608, URL http://dx.doi.org/10.1175/BAMS-88-10-1608.

Kollias, P., M. A. Miller, E. P. Luke, K. L. Johnson, E. E. Clothiaux, K. P. Moran, K. B. Widener, and B. A. Albrecht, 2007b: The atmospheric radiation measurement program cloud profiling radars: Second-generation sampling strategies, processing, and cloud data products. *Journal of Atmospheric and Oceanic Technology*, **24 (7)**, 1199–1214, doi:10.1175/JTECH2033.1, URL http://dx.doi.org/10.1175/JTECH2033.1.

Lhermitte, R., 1990: Attenuation and scattering of millimeter wavelength radiation by clouds and precipitation. *Journal of Atmospheric and Oceanic Technology*, **7 (3)**, 464–479, doi:10.1175/1520-0426(1990)007⟨0464:AASOMW⟩2.0.CO;2, URL http://dx.doi.org/10.1175/1520-0426(1990)007⟨0464:AASOMW⟩2.0.CO;2.

Li, L., and Coauthors, 2001: Retrieval of Atmospheric Attenuation Using Combined Ground-Based and Airborne 95-GHz Cloud Radar Measurements. *Journal of Atmospheric and Oceanic Technology*, **18 (8)**, 1345–1353, doi:10.1175/1520-0426(2001)018⟨1345:ROAAUC⟩2.0.CO;2, URL http://dx.doi.org/10.1175/1520-0426(2001)018⟨1345:ROAAUC⟩2.0.CO;2.

Liebe, H. J., 1985: An updated model for millimeter wave propagation in moist air. *Radio Sci.*, **20 (5)**, 1069–1089.

Ligthart, L. P., L. R. Nieuwkerk, and J. S. Vansinttruyen, Eds., 1986: *Basic characteristics of FM-CW radar systems*.

Löhnert, U., S. Crewell, C. Simmer, and A. Macke, 2001: Profiling cloud liquid water by combining active and passive microwave measurements with cloud model statistics. *Journal of Atmospheric and Oceanic Technology*, **18 (8)**, 1354–1366, doi:10.1175/1520-0426(2001)018⟨1354:

PCLWBC⟩2.0.CO;2, URL http://dx.doi.org/10.1175/1520-0426(2001)018⟨1354:PCLWBC⟩2.0.CO;2.

Luke, E., P. Kollias, and M. D. Shupe, 2010: Detection of supercooled liquid in mixed-phase clouds using radar Doppler spectra. *J. Geophys. Res.*, **115 (D19201)**, doi:10.1029/2009JD012884.

Maier, F., J. Bendix, and B. Thies, 2012: Simulating Z–LWC Relations in Natural Fogs with Radiative Transfer Calculations for Future Application to a Cloud Radar Profiler. *Pure and Applied Geophysics*, doi:10.1007/s00024-011-0332-0.

Matrosov, S. Y., and A. J. Heymsfield, 2000: Use of Doppler radar to assess ice cloud particle fall velocity-size relations for remote sensing and climate studies. *J. Geophys. Res.*, **105**, 22 427–22 436, doi:10.1029/2000JD900353.

Moran, K. P., B. E. Martner, M. J. Post, R. A. Kropfli, D. C. Welsh, and K. B. Widener, 1998: An unattended cloud-profiling radar for use in climate research. *Bulletin of the American Meteorological Society*, **79 (3)**, 443–455, doi:10.1175/1520-0477(1998)079⟨0443:AUCPRF⟩2.0.CO;2, URL http://dx.doi.org/10.1175/1520-0477(1998)079⟨0443:AUCPRF⟩2.0.CO;2.

O'Connor, E. J., R. J. Hogan, and A. J. Illingworth, 2005: Retrieving Stratocumulus Drizzle Parameters Using Doppler Radar and Lidar. *Journal of Applied Meteorology*, **44 (1)**, 14–27, doi:10.1175/JAM-2181.1, URL http://dx.doi.org/10.1175/JAM-2181.1.

Protat, A., J. Delanoë, D. Bouniol, A. J. Heymsfield, A. Bansemer, and P. Brown, 2007: Evaluation of ice water content retrievals from cloud radar reflectivity and temperature using a large airborne in situ microphysical database. *Journal of Applied Meteorology and Climatology*, **46 (5)**, 557–572, doi:10.1175/JAM2488.1, URL http://dx.doi.org/10.1175/JAM2488.1.

Sami, G., 2009: Radio Wave Propagation Characteristics in FMCW Radar. *Journal of Electromagnetic Analysis and Applications*, **1 (4)**, 275–278, doi:10.4236/jemaa.2009.14042.

Sekelsky, S. M., 2002: Near-Field Reflectivity and Antenna Boresight Gain Corrections for Millimeter-Wave Atmospheric Radars. *Journal of Atmospheric and Oceanic Technology*, **19 (4)**, 468–477, doi:10.1175/1520-0426(2002)019⟨0468:NFRAAB⟩2.0.CO;2, URL http://dx.doi.org/10.1175/1520-0426(2002)019⟨0468:NFRAAB⟩2.0.CO;2.

Shupe, M., P.Kollias, S. Y. Matrosov, and T. L. Schneider, 2004: Deriving mixedphase cloud proper ties from Doppler radar spectra. *Journal of Atmospheric and Oceanic Technology*, **21**, 660–670.

Stephens, G. L., and Coauthors, 2002: The Cloudsat Mission and the A-Train. *Bull. Am. Meteorol. Soc.*, **83**, 1771–1790.

Thies, B., K. Müller, F. Maier, and J. Bendix, 2010: Fog monitoring using a new 94 GHz FMCW cloud radar. *5th International Conference on Fog, Fog Collection and Dew, held 25-30 July, 2010 in Münster, Germany. ¡A href="http://www.fogconference.org"¿http://www.fogconference.org¡/A¿, id.FOGDEW2010-103*, 103.

Williams, C., 2011: Inexpensive FM-CW Radar for Boundary-Layer Precipitation Studies. *Geoscience and Remote Sensing Letters, IEEE*, **8 (6)**, 1031–1035, doi:10.1109/LGRS.2011.2150733.

Wolde, M., and A. Pazmany, 2005: NRC Dual-Frequency Airborne Radar for Atmospheric Research. *32nd International Conference on Radar Meteorology*, Albuquerque, New Mexico, International Conference on Radar Meteorology.

Wood, C. R., E. J. O'Connor, R. A. Hurley, D. R. Reynolds, and A. J. Illingworth, 2009: Cloud-radar observations of insects in the UK convective boundary layer. *Meteorological Applications*, **16**, 491–500, doi:10.1002/met.146.

Yamaguchi, J., and Coauthors, 2006: Sensitivity of FMCW 95Ghz cloud radar for high clouds. *Microwave Conference, 2006. APMC 2006. Asia-Pacific*, 1841–1846, doi:10.1109/APMC.2006.4429767.

-

LIST OF TABLES

Table 1. Radar main specifications 31

Table 2. Radar characteristics for each mode 32

TABLE 1. Radar main specifications

Radar type	Bistatic FMCW, single polarisation Doppler
Operating frequency	≈94.95 GHz
Transmitter type	Solid state
System noise figure	≈8 dB
Transmit power	27 to 30 dBm (0.5 to 1 W)
Input power	550 VA
Dimensions and weight	
Weight	60-70 kg
Length	154 cm
Width	95 cm
Height	74 cm
Antenna type	2 Cassegrain-field parabolic dishes
Diameter	0.60 m
Gain	54 dBi
Beamwidth	0.4 deg
Data acquisition / processing system	ADC / FPGA
Chirp analyse time	40-80 μs
Sampling rate	51.2 MHz
Algorithm used	Pulse Pair Processing
Archive data format	netCDF
Measurements	Reflectivity and Doppler velocity
Minimun distance to valid signal	40 m (depending on resolution)

TABLE 2. Radar characteristics for each mode

Range resolution (m)	12.5	25	100	200
Unambiguous range (km)	6	12	12	12
Unambiguous velocity (m/s)	9.87	4.935	4.935	4.935
Pulse repetition period (T_{rep}) (μs)	80	160	160	160
Chirp analysis time (T_a) (μs)	40	80	80	80
Chirp band (MHz)	90 ± 12	90 ± 6	90 ± 1.5	90 ± 0.75
FFT points number	2048	4096	4096	4096
Gate number	480	480	120	60

LIST OF FIGURES

Fig. 1. Photos of the radar. Panels A and B represent a top view showing antennas and electronic and the outside of the original prototype deployed at SIRTA. Panels C, D and E show the BASTA-mobile in different positions. 34

Fig. 2. Range corrected reflectivity and Doppler velocity at 25 m resolution (3s integration). The data have collected at SIRTA from the 01/01/2015 to 23/01/2015. 35

Fig. 3. Altitude-Z distributions for the three BASTA (SIRTA/BOM/MOBILE) for different time periods. In the two first columns (panels a to f) the color scale represents the number of hit in each reflectivity and altitude bins. Panels g to l show the same distributions respectively once normalized by the total number at each altitude. The dashed line highlights the 1 km range. 36

Fig. 4. Fog/low clouds measurements, Vd is the Doppler velocity and Z is the radar reflectivity. The data were collected by BASTA-MOBILE at SIRTA from the 21st to the 23rd of December 2014 and from the 5th to the 7th of January 2015. The vertical stripes on the second examples are due to electrical power disruption, the radar restarted automatically 37

Fig. 5. Range corrected reflectivity and Doppler velocity at 12.5 m, 25 m, 100 m and 200 m resolution. The data have collected at SIRTA on the 18/01/2014. 38

Fig. 6. Example of merged data collected on the 19th of January 2014. Top panel presents the reflectivity, middle panel the Doppler velocity. Bottom panel illustrates the data source (12.5 m/25 m/100 m/200 m). 39

Fig. 7. Frequency Modulated Continuous Wave principle and an example of the impact of using half of the chirp (grey box). 40

Fig. 8. Radar block diagram 41

Fig. 9. FMCW signal processing 42

Fig. 10. Calibration approach example for BASTA SIRTA on the 25th of June 2013. The calibration is carried out using the radar pointing horizontally towards a trihedral target. Panels a and b represent the average raw reflectivity and velocity respectively as a function of radar range. Grey dashed lines represent mean ± standard deviation. Panel c illustrates the histogram of the energy backscattered by the target. 43

Fig. 11. Calibration verification using rain echo and rain rate and drop size measurements. BASTA-SIRTA is pointing vertically while BASTA-MOBILE is inclined and protected from rain. The average value of calibrated reflectivity of both radars as a function of rain rate at 306 m (vertical) and 506 m (inclined 30°) range is represented in panels a and b respectively. The red line, in panel a, represents the simulated attenuated reflectivity at 500 m, using the measured drop size distribution T-matrix calculation assuming an aspect ratio as a function of diameter (Beard and Chuang 1987). 44

Fig. 12. Comparison of the range corrected reflectivity at DARWIN (Australia) between the 35 GHz KAZR Doppler radar sensitive mode (a), normal mode (b) and the 3 BASTA modes at 25 m (c), 100 m (d) and 200 m (d) vertical resolution. Panels f) and g) show the mean profiles for each radar and modes between 12 UTC and 13 UTC and between 14.5 UTC and 15.5 UTC. The dashed lines represent the noise level for each profile. 45

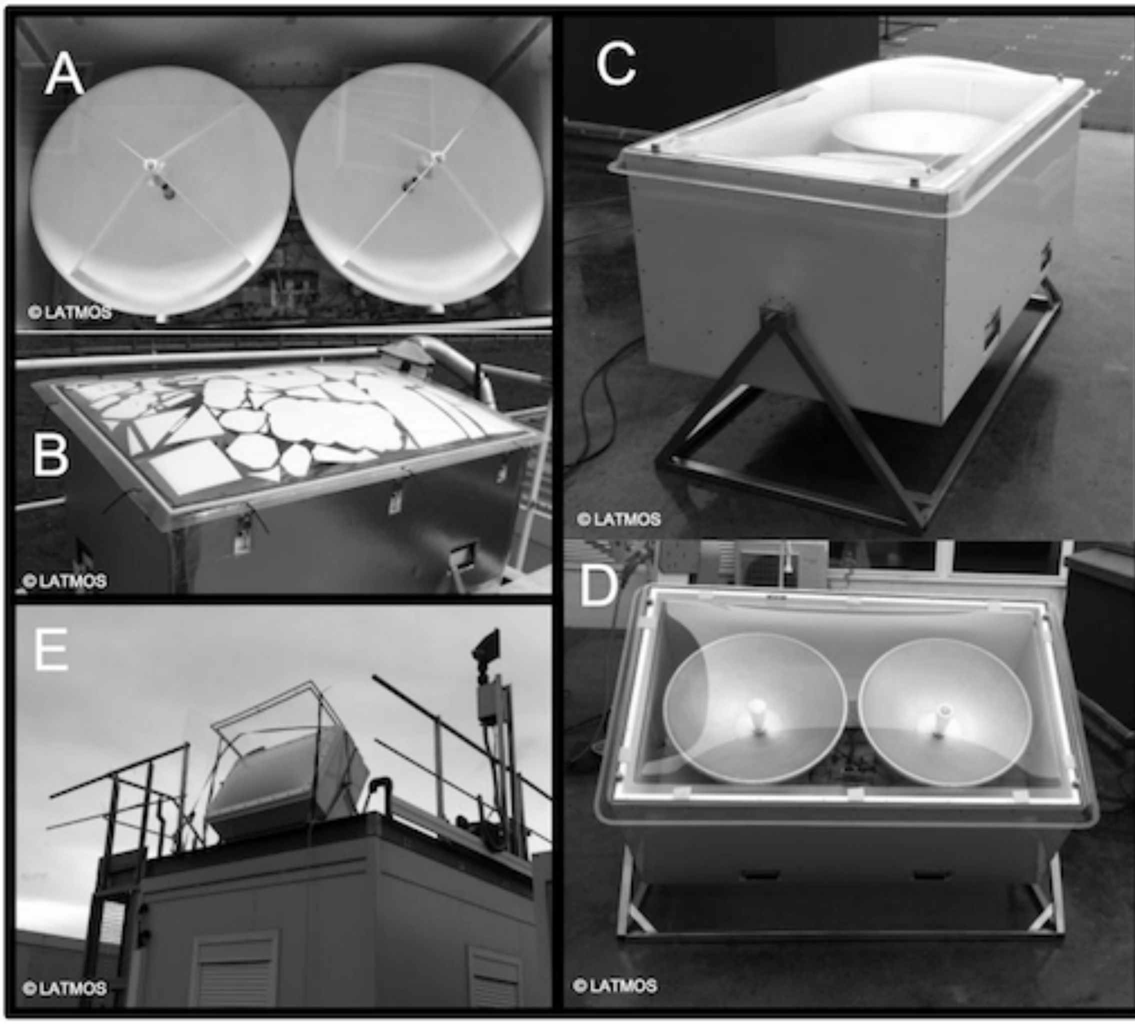

FIG. 1. Photos of the radar. Panels A and B represent a top view showing antennas and electronic and the outside of the original prototype deployed at SIRTA. Panels C, D and E show the BASTA-mobile in different positions.

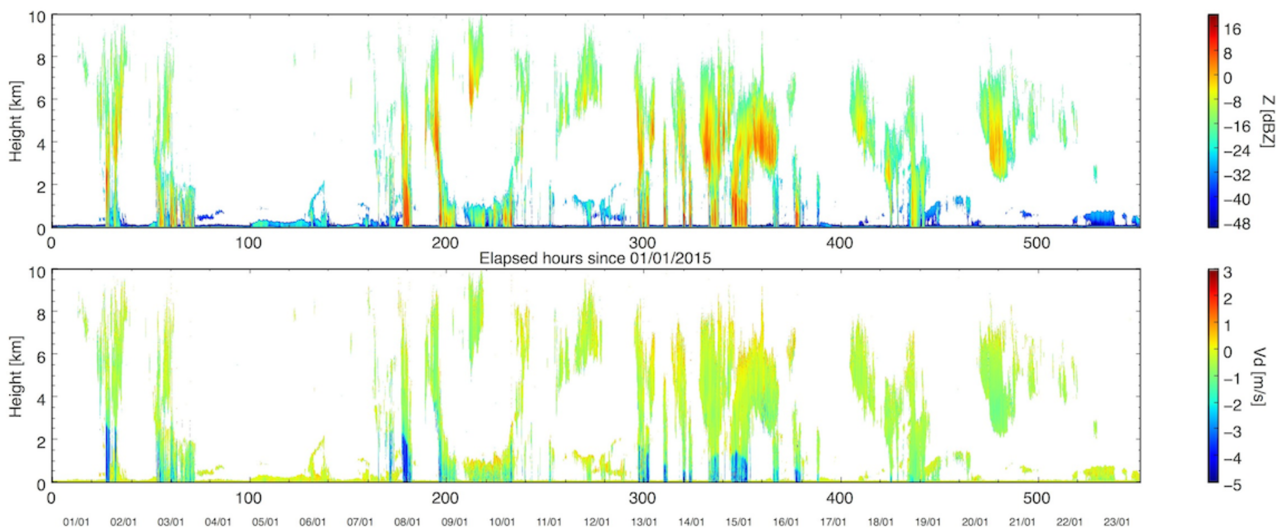

FIG. 2. Range corrected reflectivity and Doppler velocity at 25 m resolution (3s integration). The data have collected at SIRTA from the 01/01/2015 to 23/01/2015.

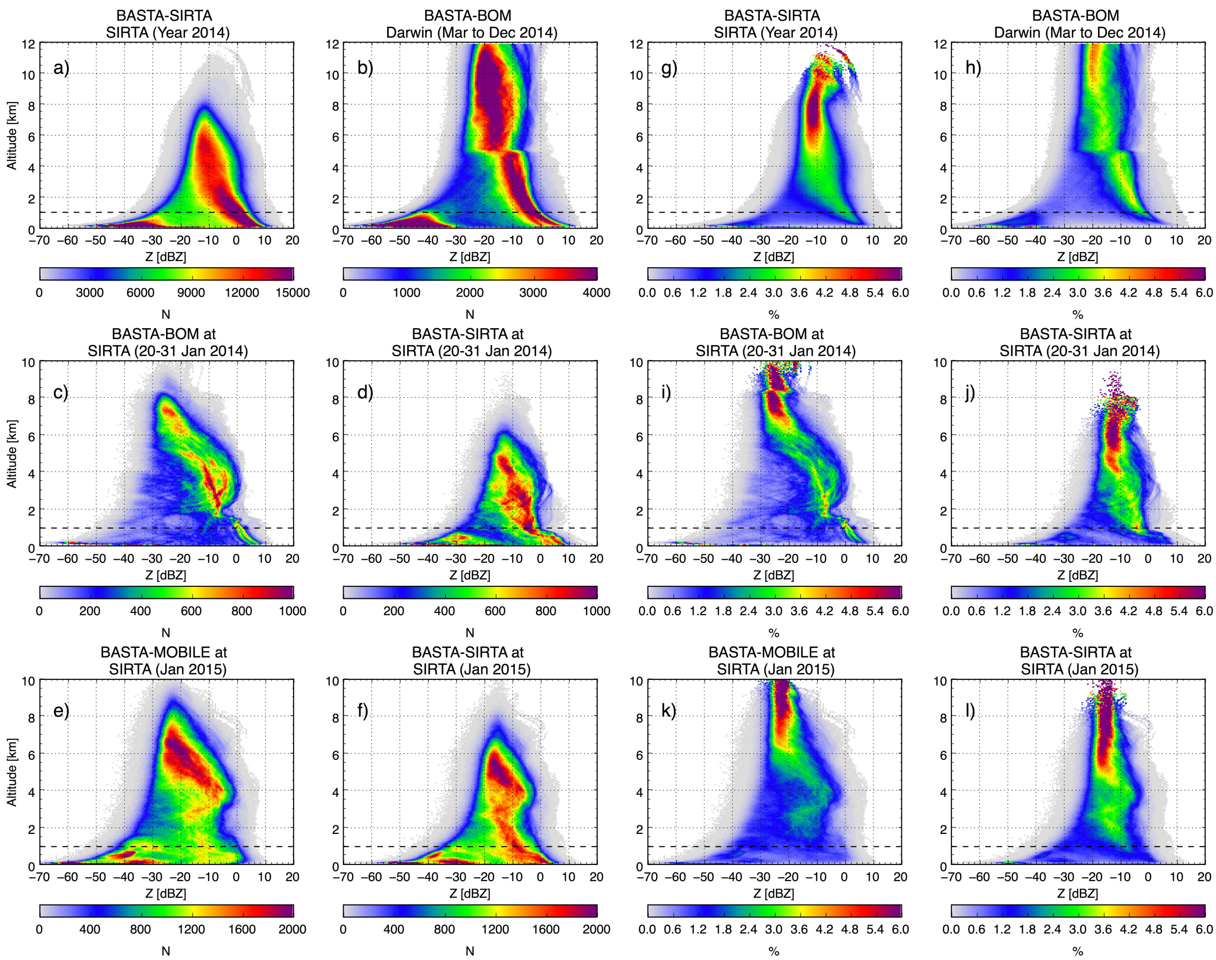

648 FIG. 3. Altitude-Z distributions for the three BASTA (SIRTA/BOM/MOBILE) for different time periods. In the two first columns (panels a to f) the color scale represents the number of hit in each reflectivity and altitude bins. Panels g to l show the same distributions respectively once normalized by the total number at each altitude. The dashed line highlights the 1 km range.

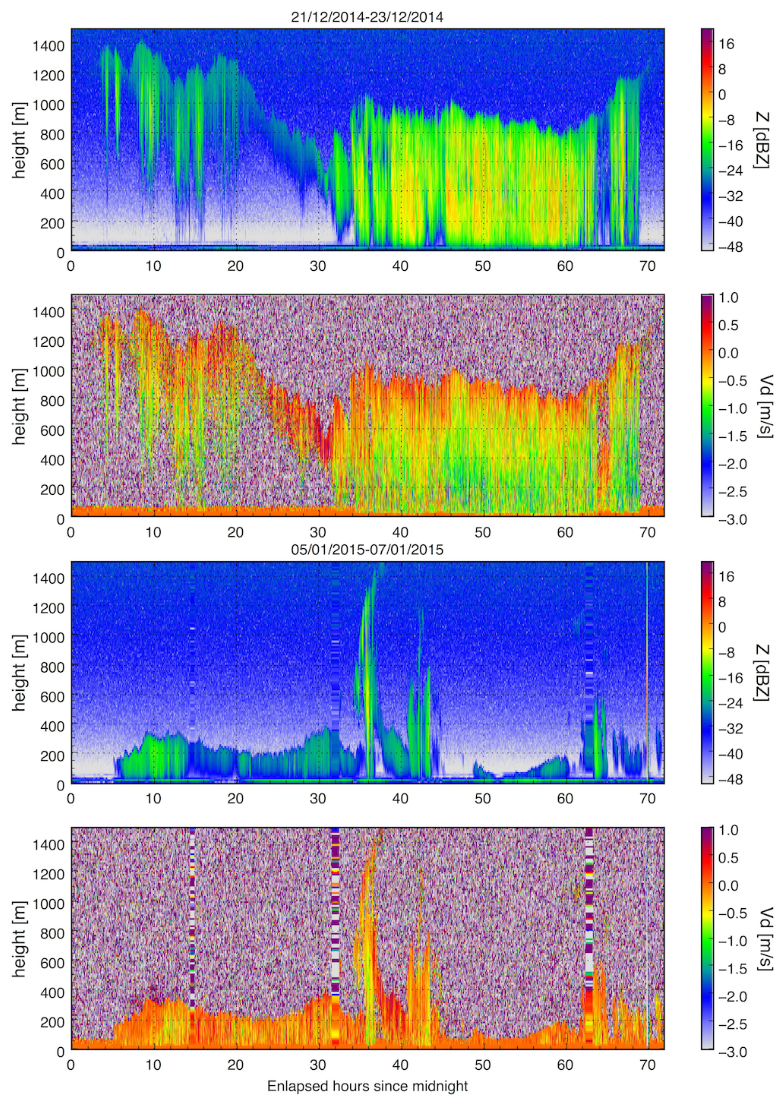

FIG. 4. Fog/low clouds measurements, Vd is the Doppler velocity and Z is the radar reflectivity. The data were collected by BASTA-MOBILE at SIRTA from the 21st to the 23rd of December 2014 and from the 5th to the 7th of January 2015. The vertical stripes on the second examples are due to electrical power disruption, the radar restarted automatically

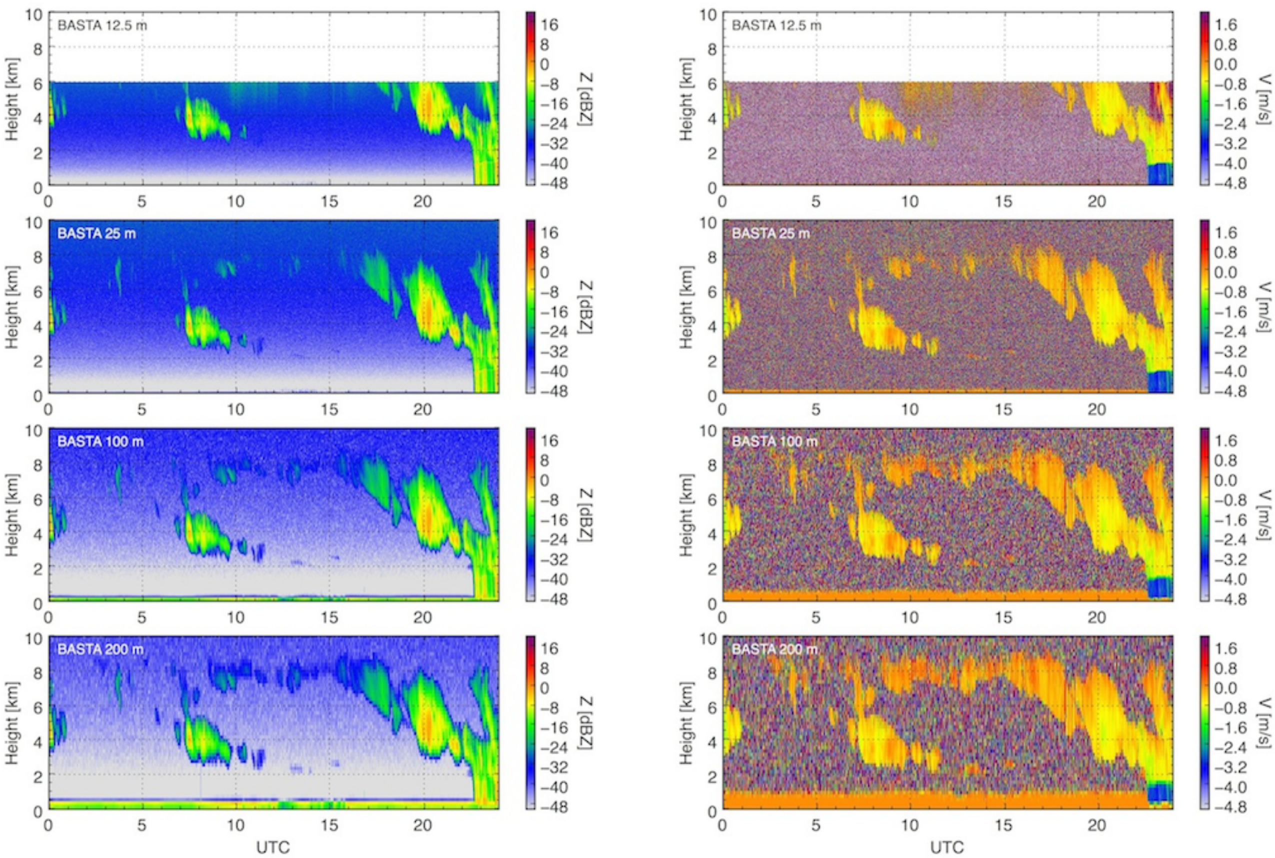

656 FIG. 5. Range corrected reflectivity and Doppler velocity at 12.5 m, 25 m, 100 m and 200 m resolution. The data have collected at SIRTA on the 18/01/2014.

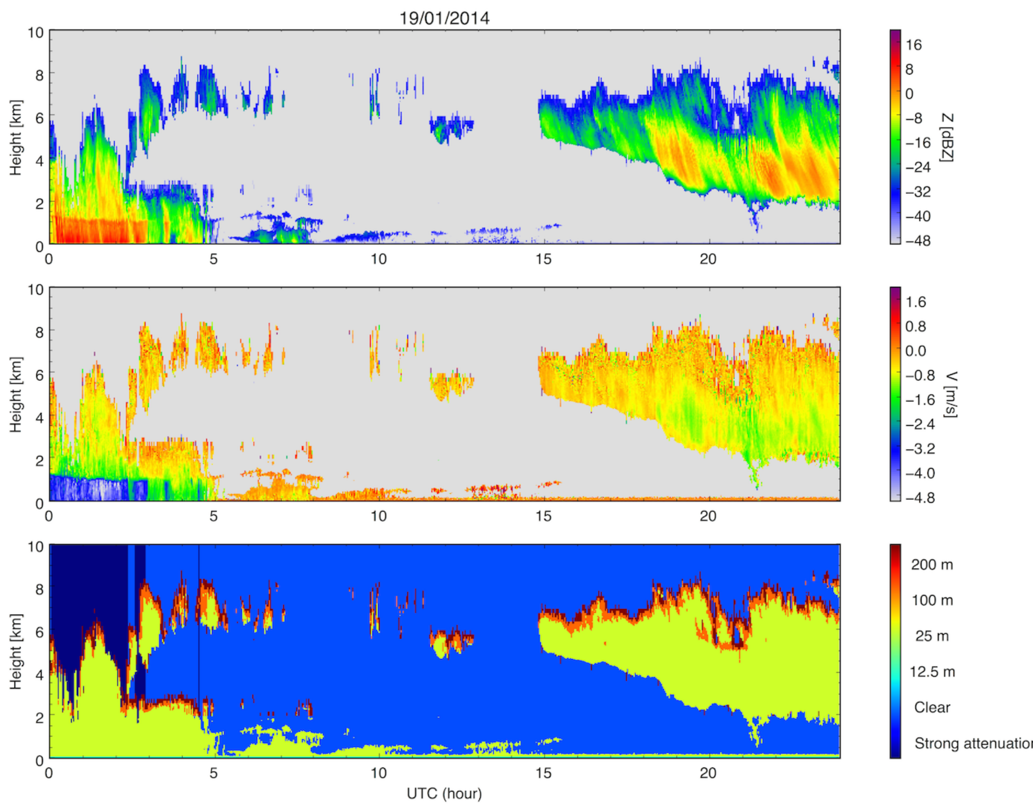

658 FIG. 6. Example of merged data collected on the 19th of January 2014. Top panel presents the reflectivity,
659 middle panel the Doppler velocity. Bottom panel illustrates the data source (12.5 m/25 m/100 m/200 m).

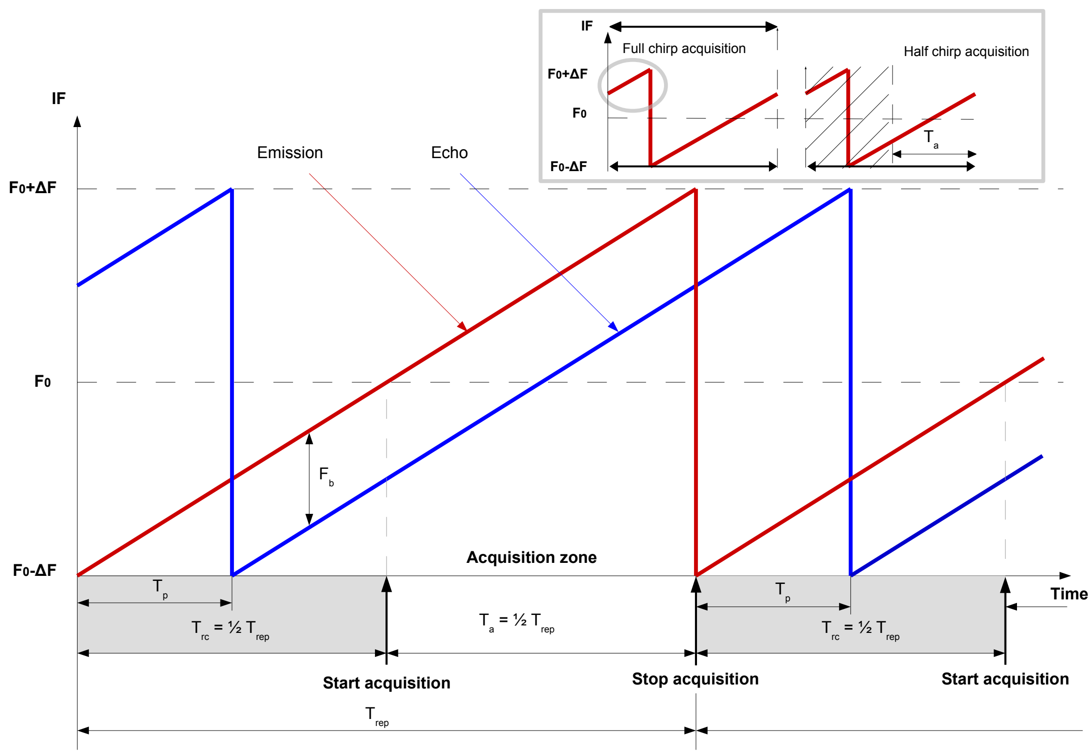

660 FIG. 7. Frequency Modulated Continuous Wave principle and an example of the impact of using half of the
661 chirp (grey box).

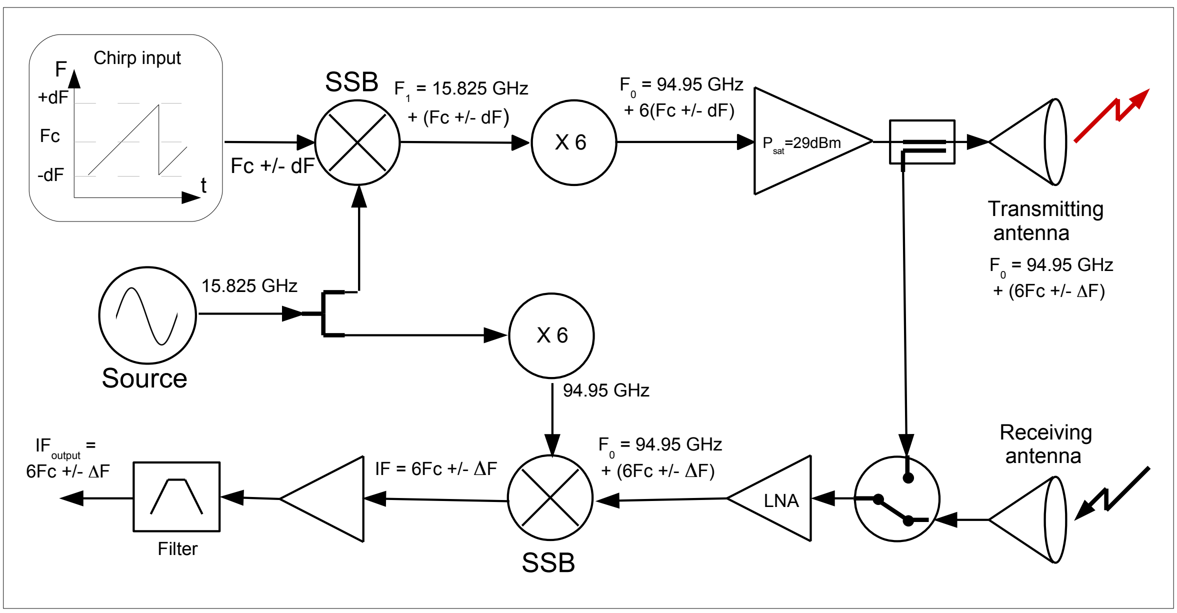

FIG. 8. Radar block diagram

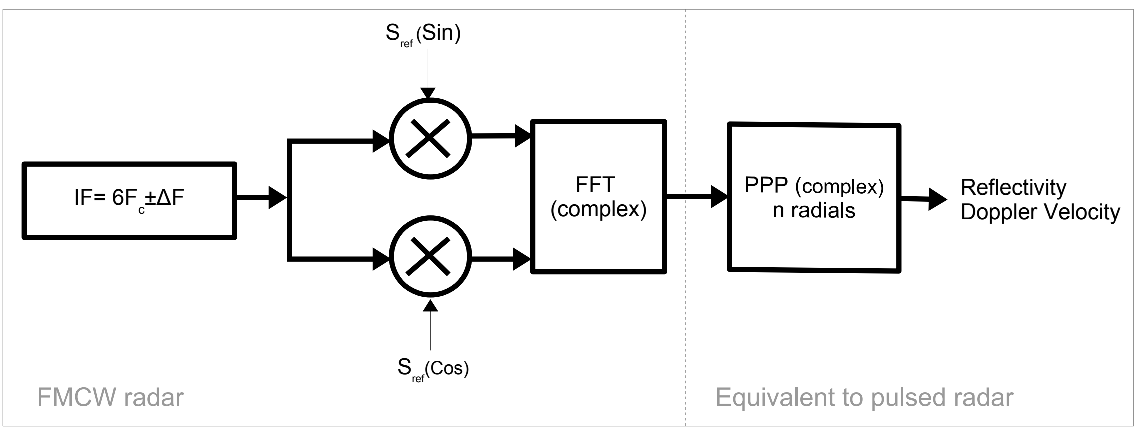

FIG. 9. FMCW signal processing

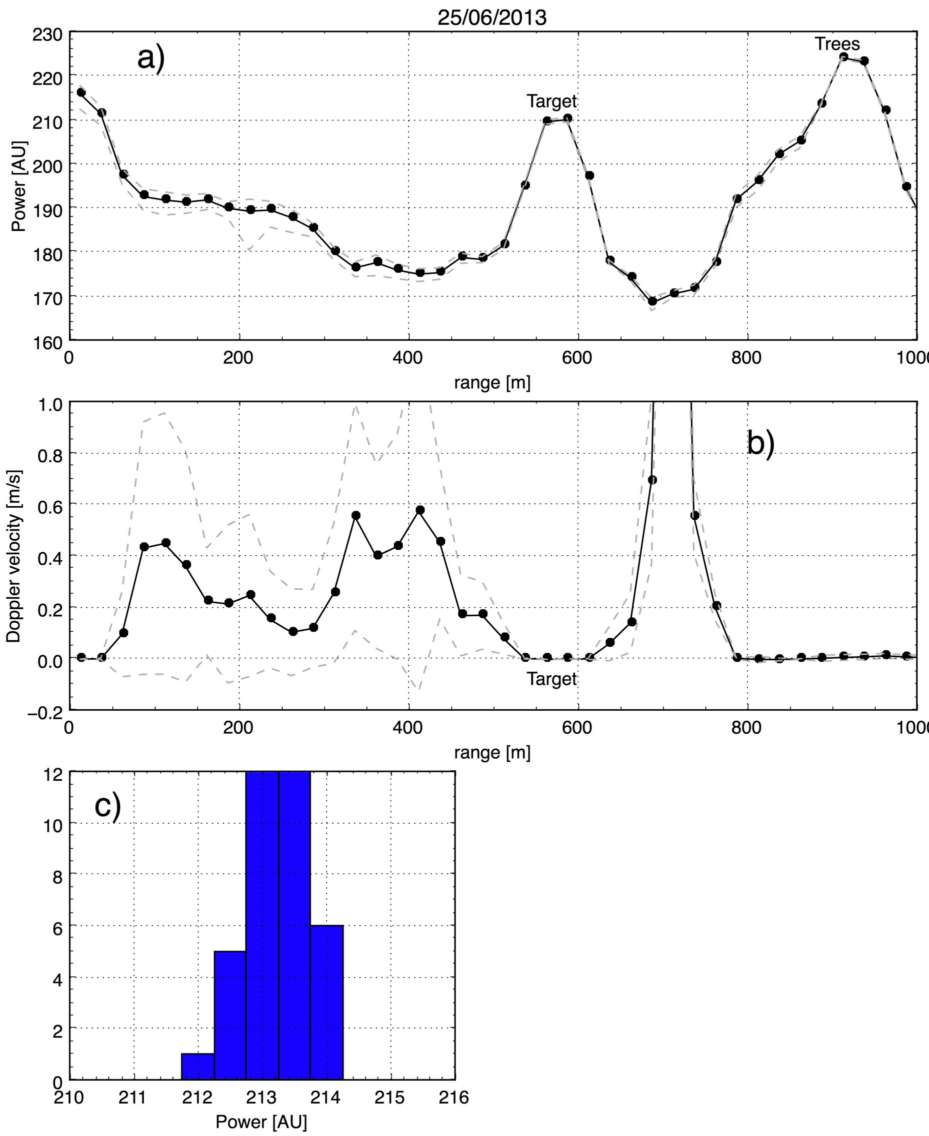

FIG. 10. Calibration approach example for BASTA SIRTA on the 25th of June 2013. The calibration is carried out using the radar pointing horizontally towards a trihedral target. Panels a and b represent the average raw reflectivity and velocity respectively as a function of radar range. Grey dashed lines represent mean $\pm$ standard deviation. Panel c illustrates the histogram of the energy backscattered by the target.

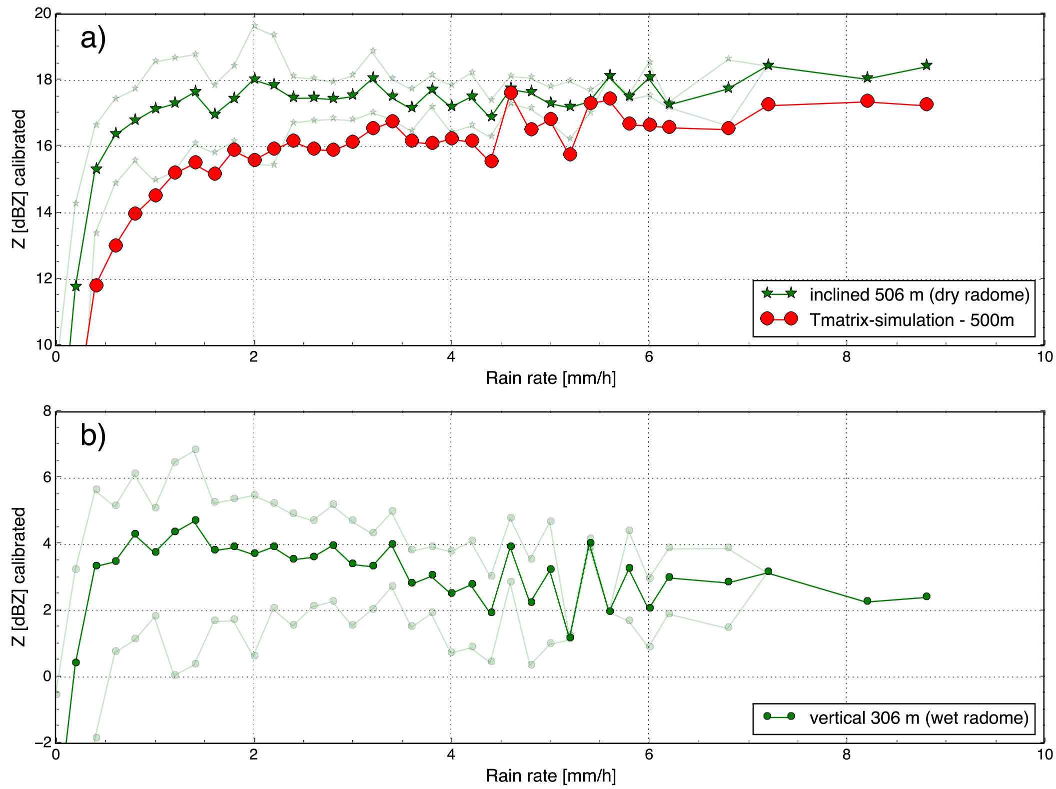

FIG. 11. Calibration verification using rain echo and rain rate and drop size measurements. BASTA-SIRTA is pointing vertically while BASTA-MOBILE is inclined and protected from rain. The average value of calibrated reflectivity of both radars as a function of rain rate at 306 m (vertical) and 506 m (inclined 30°) range is represented in panels a and b respectively. The red line, in panel a, represents the simulated attenuated reflectivity at 500 m, using the measured drop size distribution T-matrix calculation assuming an aspect ratio as a function of diameter (Beard and Chuang 1987).

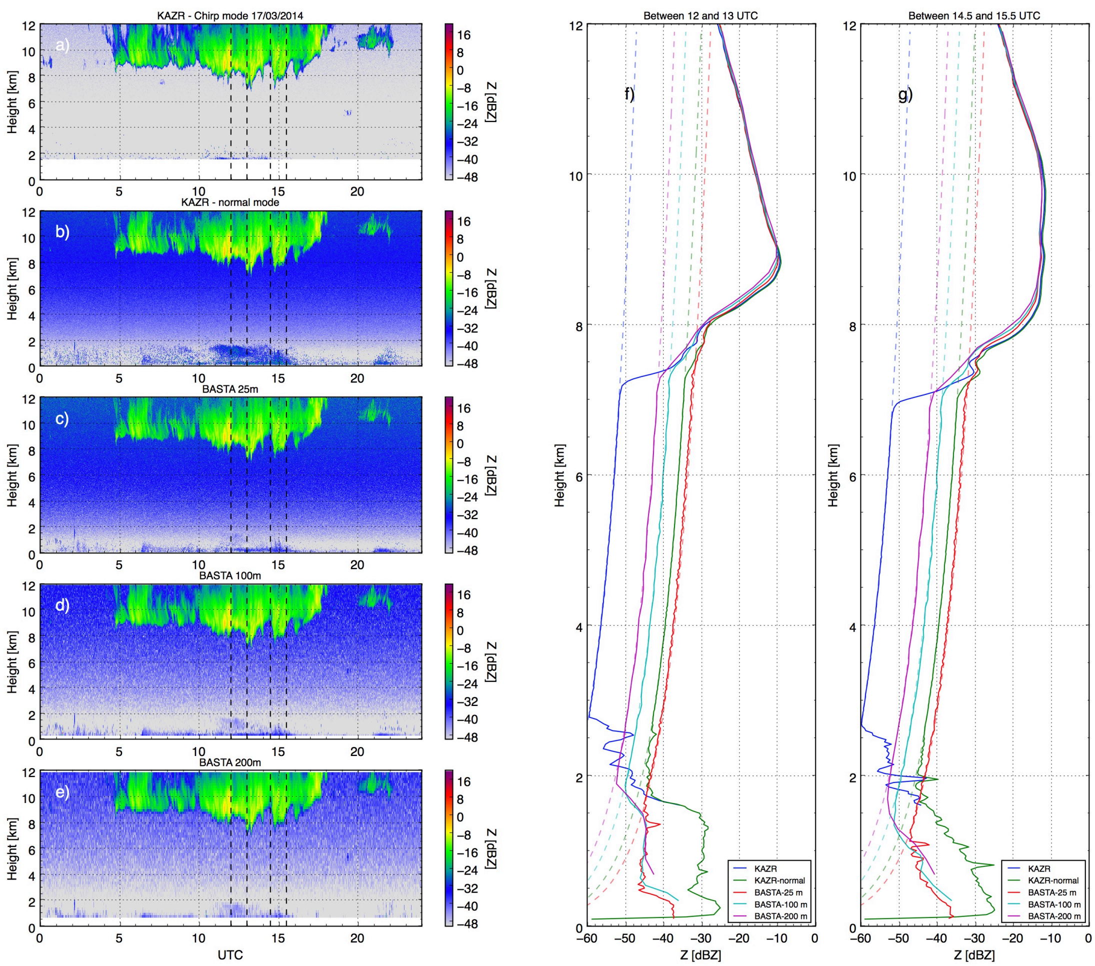

672 FIG. 12. Comparison of the range corrected reflectivity at DARWIN (Australia) between the 35 GHz KAZR Doppler radar sensitive mode (a), normal mode (b) and the 3 BASTA modes at 25 m (c), 100 m (d) and 200 m (d) vertical resolution. Panels f) and g) show the mean profiles for each radar and modes between 12 UTC and 13 UTC and between 14.5 UTC and 15.5 UTC. The dashed lines represent the noise level for each profile.